http://ansinet.com/itj

ITJ

ISSN 1812-5638

# INFORMATION TECHNOLOGY JOURNAL

ANSInet
Asian Network for Scientific Information
308 Lasani Town, Sargodha Road, Faisalabad - Pakistan

Information Technology Journal 12 (4): 664-671, 2013
ISSN 1812-5638 / DOI: 10.3923/itj.2013.664.671


# Study on Voltage-stabilizing Control of ICPT System

Yuanfu Wu, Yue Sun, Yong Tian, Fangxun Yang and Yugang Su
College of Automation, Chongqing University, Chongqing 400030, China

**Abstract:** As nonlinear switch unit leads to higher-order switch nonlinear behavior, it is difficult to build an accurately model and control the output voltage of the ICPT system. To address this problem, this study presents a neural network-based control strategy to stabilize the secondary output voltage. This strategy makes full use of the nonlinear function approximation of the neural network. To converge the neural network, a multi-layered feedforward neural network based on back-propagation algorithm has been designed via learning train samples. Besides, to ensure the stability of output power, the neural network controller has been employed to stabilize the secondary output voltage by regulating the input voltage. Finally, simulations and experimental results have verified that this control strategy is feasible.

**Key words:** Neural network, voltage-stabilizing control, inductively coupled power transfer, back-propagation algorithm

## INTRODUCTION

Inductively Coupled Power Transfer (ICPT) technology is a new mode of power supply, which utilizes high frequency magnetic fields to transmit power from the source to the receiver in the form of electrical isolation (Cannon *et al*., 2009; Valtchev *et al*., 2009; Sun *et al*., 2012). It effectively solves the seamless access problem and changes traditional supply mode that transmit power directly via electric conductor. ICPT technology has extensive application prospects in various industries, such as manufacturing (Moradewicz and Kazmierkowski, 2010), medicine (Madawala and Thrimawithana, 2011) and electric vehicles (Tian *et al*., 2012) since it is environmental friendly, convenient and flexible.

An ICPT system has a primary side and a secondary side. When the secondary impedance varies, the reflected impedance will be introduced in the primary coil due to the electromagnetic coupling effect. Hence, the primary exciting current will decrease and the operating frequency of Zero Voltage Switching (ZVS) will drift (Hu *et al*., 2000), which weakens the capability of transmission power and reduces the transmission efficiency. If the frequency drift is too large, multi-cycle working points phenomenon will appear and cause big influence on operational stability of system. When the frequency offsets the inherent frequency and the primary input voltage remains constant, the pickup voltage will drop sharply and generate bigger fluctuation, causing hidden danger for the normal load operations (Li *et al*., 2012). Therefore, to ensure the operational stability of system and to improve its transmission efficiency, it is important to stabilize the secondary output voltage.

Current control strategies for the secondary output voltage are mainly based on the primary phase-shifted control (Yugang *et al*., 2008), the primary detuning control (Si *et al*., 2008) and the primary energy injection control (Li *et al*., 2009). Although no auxiliary circuit is needed for the primary phase-shifted control as it regulates the voltage via flexible power switches to change the phase-shift angle, the switching loss and switching stress increases because of the hard switching mode. As for the primary detuning control, its demand for an auxiliary circuit not only increases the control difficulty and system weight but also reduces the total efficiency. Besides, the primary energy injection control will cause sharp decrease of frequency when the system is in light running, not to mention that only when the pickup voltage is higher than the regulated voltage needed, the output voltage of ICPT system can be regulated via utilizing the decoupling method for the short circuit of auxiliary coil.

In addition, the ICPT system usually presents complex higher-order switch nonlinear behavior, for it comprises a number of nonlinear switching devices and energy storage components. Hence, modeling and control design are rather complex, particularly when the dynamic behavior of ICPT system is under the action of external disturbance. By contrast, neural network control doesn't rely on accurate mathematical model of system and it reflects complex nonlinear objects that are difficult to describe accurately at arbitrary precision (Coban, 2004; Bigdeli *et al*., 2008; Keshavarzi *et al*., 2012). Thus, neural network control is entitled to the abilities of learning and adaptation, as well as practical value in the applied control system.

**Corresponding Author:** Yong Tian, College of Automation, Chongqing University, Chongqing 400030, China

Based on the review above, this study proposes a neural work-based control strategy to stabilize the secondary output voltage of ICPT system. During the control period, the system will work in the soft-switching mode and utilize nonlinear function approximation character of the neural network to build a neural network-based control model when the system gains input disturbance and load step. This model will then dynamically regulate the primary input DC voltage by detecting the actual secondary output voltage, and thus it will keep the secondary voltage at the desired value. Finally, simulation and experimental results have verified the feasibility of this neural work-based control strategy to stabilize output voltage of the ICPT system.

## IMPROVED π-TYPE ICPT SYSTEM

Figure 1 shows the circuit topology of an ICPT system with improved π-type resonant link. Similar to traditional ICPT system, it also consists of the primary and the secondary sides. At the primary side, a quasi-current source is built on the input DC source $E_{dc}$ and the filter inductance $L_d$, while a high frequency energy conversion link is made of two power switch pairs ($S_1$, $S_4$) and ($S_3$, $S_2$). Therefore, the forward and backward energy injection modes can be triggered by alternating break-over of the switch pairs. When the power switch pairs are switched at the zero-crossing of capacitor voltage, a ZVS operation would be realized in the system. At this moment, the effective value of the capacitor voltage $u_p$ can be calculated by:

$$U_p = \frac{\pi E_{dc}}{2\sqrt{2}} \quad (1)$$

In this system, capacitor $C_b$ and inductance $L_b$ form the bias network as an improved part of the π-type series-parallel resonant circuit (Dai *et al*., 2010), which eliminates the harmonic distortion, improves the resonant quality of system and operation stability, increases the rated power of reactive circulating-current, reduces the dynamic effect caused by parameter uncertainty of system and load switching, and eliminates the EMI interference. The bias inductance and capacitor are shown below:

$$\begin{cases} I_{Lb} = I_{cb} = i_{Lp} \times m \\ L_b = L_n / m \\ C_b = C_{n1} \times m \end{cases} \quad (2)$$

where, m is the bias facto, $I_{Lb}$ is the current across the bias inductance, $I_{Cb}$ is the current on the bias capacitor.

$C_p$ and $L_p$ comprise the series high frequency resonant link. The sinusoidal exciting current with low distortion degree is produced at the primary side. According to the electromagnetic induction principle, the high frequency sinusoidal power is transferred from the transmitter to the pickup by mutual inductance M.

At the secondary side, the parallel resonant network with the same frequency at the primary side includes the capacitor $C_s$ and the receiver coil $L_s$. The output high frequency power $u_{cs}$ realizes the bidirectional rectification of high frequency sinusoidal current by uncontrollable rectifier full bridge. As the filter choke of the rectifier bridge, $L_f$ filters out the high frequency AC current effectively, and only allows low frequency AC current and DC current to pass. Then, the power across the choke is output on the load $R_L$.

## THE VOLTAGE-STABILIZING CONTROL STRATEGY OF ICPT SYSTEM

To get the main factor which influences the secondary output voltage, rectifier link, filter link and load resistance $R_L$ can be equivalent to the equivalent resistance $R_{eq}$, as shown in Fig. 2, while the power losses of rectifier and filter link in the secondary are ignored.

The total impedance of the secondary coil is shown in Eq. 3:

$$Z_s = \frac{1}{1/R_{eq} + j\omega C_s} + j\omega L_s \quad (3)$$

The reflected impedance from the secondary to the primary is shown in Eq. 4:

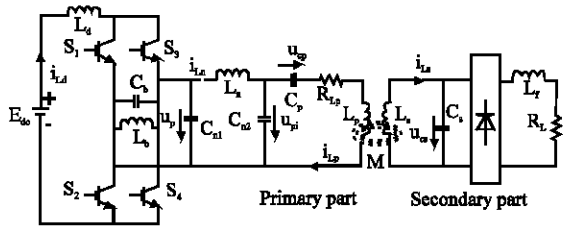


Fig. 1: The circuit topology of π-type ICPT system

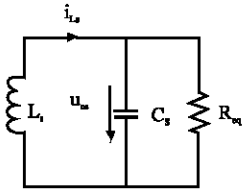

Fig. 2: Equivalent mode of the secondary side

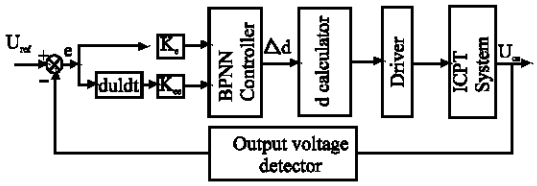


Fig. 3: Control configuration

$$Z_s=\frac{\omega^2M^2}{Z_s}=\frac{\omega^2M^2}{j\omega L_s+\dfrac{1}{j\omega L_s+1/R_{eq}}} \quad (4)$$

Equation 4 shows that the reflected impedance varies with the equivalent resistance $R_{eq}$ which will lead to the drift of primary resonant current. In this case, the input voltage value is changed dynamically to meet the requirement of secondary output power. Hence, an output voltage-stabilizing control strategy based on the Back Propagation (BP) neural network is proposed. Its core mechanism is as follows: When the voltage-stabilizing $U_{ref}$ is set, error rate and error change rate are collect by comparing detected practical output voltage and referenced voltage as sample data to input into the neural network control. Meanwhile, the system is driven by the variation module of duty cycles whose output power switches are transformed as a controller. Consequently, a closed loop control system is formed to dynamically stabilize the output voltage on the condition of parameter disturbance and load step. The control configuration is shown in Fig. 3.

## BP NEURAL NETWORK MODEL

The BP neural network is a multi-layered feedforward network with unidirectional propagation (Eriki and Udegbunam, 2008; Hsieh, 2010). It is the core of forward networks and the essence of artificial neural networks. It's named as the BP neural network, for it uses the errors back propagation algorithm which modifies the connection weights and thresholds of each output and input layers to reduce the difference between target output and practical output. The BP neural network is made of an input layer, a single or multiple hidden layers and an output layer. There is no connection among neurons at the same layers but neurons from different layers are connected with their next layer. According to the approximation theory of neural network, in the case of reasonable hidden neuron numbers, any nonlinear complex function with limited discontinuous points can be approximated at an arbitrary precision. As a nonlinear modeling method, it has favorable fitting precision,

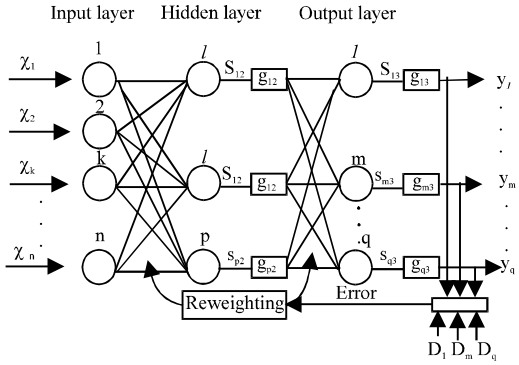


Fig. 4: Structure of a generalized three-layered BP neural network

nonlinear quality and generalization ability (Abdalla and Deris, 2005; Dutta *et al*., 2012).

A generalized three-layered feedforward network is shown in Fig. 4. This network includes neurons like 'n' as the input layer, 'p' as the hidden layer, and 'q' as the output layer.

Assuming the input vector of neural is $X = [x_1, x_2,\ldots x_k,\ldots,x_n]$ and the output vector is $Y = [y_1,\ldots,y_m,\ldots,y_q]$. As the selection of excitation function through the hidden layer to the output layer has significant influence on the network performance and learning speed S-type activation function is used in the current model due to it resembles to the input-output features of human brain and thus has ideal bionic effects. As shown in Fig. 4, module g is the S-type activation function and the first floor has no activation function. Taking the output neuron m as an example to show how this neural network works. Assuming its input weight is $W_{lm.3}$ and its value is calculated based on the signal $g_{l2}$ from Neuron 1. The square of the difference $e_m$ between the practical output $y_m$ and the target value $D_m$ is defined as the index function of this neural network algorithm, as shown in Eq. 5:

$$e^2{}_m=\left(D_m-y_m\right)^2 \quad (5)$$

Based on gradient descent, the modifier formula of weight coefficient between output layer node m and hidden layer node 1 is shown below:

$$\Delta W_{lm.3}=-\eta\frac{\partial e^2{}_m}{\partial W_{lm.3}} \quad (6)$$

where, $\eta>0$ is the learning rate and usually remains at a small constant value. Then the online adjustment law of network weights can be obtained by:

$$\begin{aligned}\Delta W_{lm.3} &= -\eta\frac{\partial e_m^2}{\partial W_{lm.3}}\\ &= -\eta\frac{\partial e_m^2}{\partial g_{m.3}}\frac{\partial g_{m.3}}{\partial S_{m.3}}\frac{\partial S_{m.3}}{\partial W_{lm.3}}\\ &= 2\eta(D_m - y_m)\frac{\partial}{\partial S_{m.3}}(\frac{1}{1+e^{-aS_{m.3}}})g_{l.2}\\ &= 2a\eta(D_m - y_m)y_m(1-y_m)g_{l.2}\end{aligned} \quad (7)$$

where, S-type excitation function is shown in Eq. 8:

$$f(n) = \tanh n = \frac{1-e^{-2n}}{1+e^{-2n}} \quad (8)$$

The signal $S_{m3}$ is determined by all signals from input to the neuron m, as shown in Eq. 9:

$$S_{m.3} = \sum_{l=1}^{p} W_{lm.3}g_{l.2} \quad (9)$$

The online network weight adjustment is shown in Eq. 10:

$$\begin{aligned}W_{lm.3}(k) &= W_{lm.3}(k-1) + \Delta W_{lm.3}\\ &= W_{lm.3}(k-1) + 2a\eta(D_m - y_m)y_m(1-y_m)g_{l.2}\end{aligned} \quad (10)$$

where, k is the iteration times.

So far, it has been shown that the BP algorithm is a kind of static optimization learning algorithm with gradient descent, which modifies the weights in the opposite direction of the gradient of error performance function without consideration of accumulation of previous experiences. Hence, the BP algorithm has some defects. For example, if parameters are not set properly, the neural network may oscillate during the training process, and slow down error elimination, or make the system sank into local extremum. Therefore, to improve the standard BP algorithm, this paper uses the momentum BP algorithm instead. This algorithm can decrease modification value to ensure that modification is moving towards the convergence direction in case over-modification happens during the training process. Besides, the momentum of BP algorithm usually speeds up the modification at the same gradient direction (Mao *et al*., 2007; Chen *et al*., 2010). When adjusting weights with the BP algorithm, momentum factor increases so as to filter out the high frequency oscillation generated during the training process, thus training time is shortened, but the learning rate and astringency is improved. The regulation formula is shown in Eq. 11:

$$\begin{cases}W(k) = W(k-1) + \eta[(1-\alpha)D(k-1) + \alpha D(k-2)]\\ D(k) = -\partial J/\partial w(k), \quad 0 \le \alpha < 1\end{cases} \quad (11)$$

where, w(k) is connection weight vector, D(k) is the negative gradient at k time, and a is the momentum factor. As the added momentum term is equivalent to the damping term, the tendency to oscillate will decrease during the learning process.

## DESIGN OF THE BP NEURAL NETWORK CONTROLLER

A three-layered feedforward neural network is designed in this section, where the input layer has two neurons, corresponding to the voltage error e and its change rate $e_c$ of the pickup coil; the output layer has one neuron, corresponding to the change rate of duty cycle. The amount of hidden layers and their neuron influence the functional approximation of the network. Nevertheless, the more hidden layers and hidden neurons, the longer the training time and the lower fault tolerance. Thus, the value function evaluating the BP neural network performance may not be optimal unless the number of hidden neurons is calculated based on the empirical formula:

$$n_l = \sqrt{n_j + n_l} + \kappa$$

where $n_j$ is the number of input neurons, $n_l$ is the number of output neurons, and k is the random integer from [1,10]. Thus, the number of hidden neurons should be limited to [2, 12]. To find the optimal number of hidden neurons, a BP network with variable numbers of hidden neurons is designed, then the error size with experiments is compared, and ten is found as the optimal number. The vector of the outputs of each neural node in the hidden layers is defined as [$O_3$ $O_4$,…, $O_{12}$ ], while the output of BP network is defined as $O_{13}$. The hyperbolic tangent S-type function is used to as the excitation function for the input layer to hidden layers, while "tansig" and linear excitation function "purelin" is used for hidden layers to the output layer. The learning rate is set to 0.05, maximum training times is 500 and target error is 0.000001. The output vector of hidden layers is shown in Eq. 12:

$$\begin{bmatrix}o_3\\o_4\\\vdots\\o_{12}\end{bmatrix} = \tanh\left\{\begin{bmatrix}w_{13} & w_{23}\\w_{14} & w_{24}\\\vdots & \vdots\\w_{112} & w_{212}\end{bmatrix}\begin{bmatrix}e\\ec\end{bmatrix} + \begin{bmatrix}b_3\\b_4\\\vdots\\b_{12}\end{bmatrix}\right\} \quad (12)$$

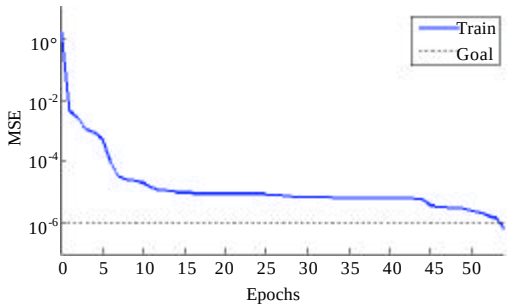


Fig. 5: Mean squared error (MSE) curve of training

The output vector of network is shown in Eq. 13:

$$o_{13} = \text{purelin}\left\{[w_{313}\, w_{413} \cdots w_{1213}]\begin{bmatrix} o_3 \\ o_4 \\ \vdots \\ o_{12} \end{bmatrix} + b_{13}\right\} \quad (13)$$

As it has shown above, when the value of the input vector is known, the practical output of the network can be figured out based on the adjustment law of weight coefficients.

Therefore, this paper uses the MATLAB neural network toolbox function to establish an untrained three-layer BP neural network, and construct input (e and $e_c$) training sample set and output ($\Delta d$) target set based on the simulation results of the ICPT system. The selected training function is the momentum BP algorithm (Traingdm). The selected weight adjustment law is the gradient descent learning function with momentum (Learngdm). The number of training time is set and then the BP network is trained off-line. The value function is used to evaluate whether the neural network training is optimal or not. The Mean Square Error (MSE) of the performance function is selected as the value function to evaluate the network's performance. The MSE curve during training is shown in Fig. 5.

Figure 5 demonstrates that MSE curve meets the requirement of target error in the 54th iteration and the designed neural network has fast convergence which approximates for the complex nonlinear functional relations of input and output with certain degree of precision.

## ANALYSIS OF SIMULATION RESULT

In the MATLAB simulation environment, the simulation circuit in Fig. 6 was established according to the control structure in Fig. 3. The effect of voltage-stabilizing control on the condition of input disturbance and load change will be discussed.

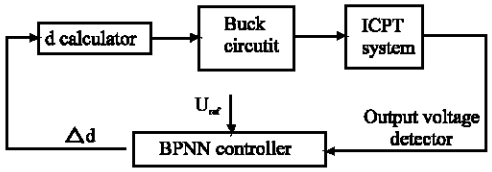


Fig. 6: Simulation model of process

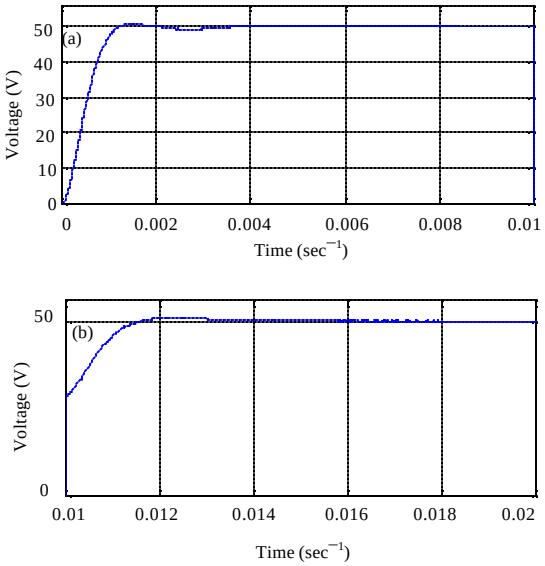


Fig. 7: Output voltage under load disturbance

The system detected the secondary output voltage in real-time and compared it with the reference voltage to get the error and its change rate as the input sample data for the neural network controller. Meanwhile, the output of the neural network had been in duty cycle variation and served as the duty cycle of Buck circuit to regulate voltage. Hence, the Buck circuit adjusted the trans formation link and then the input voltage of the ICPT system. Table 1 shows the simulation parameter values.

The system started simulation from the steady state, with the simulation time being 0.02 sec, the expected voltage-stabilizing being 50 V. The load value was changed from 30 to 20 Ω at t = 0.01 sec. Figure 7 shows the simulation waveforms of the neural network controller under load disturbance, where the output voltage of the ICPT system becomes steady after an overshoot of 0.003 sec and the voltage stays within the range of ±0.4 V during the adjustment process. The nether

Table 1: Simulation parameters of the ICPT system

| Parameter | Value |
|---|---|
| Input voltage $E_{dc}$ (V) | 200 |
| Filter inductance $L_a$ (μH) | 50 |
| Primary capacitor $C_p$ (μF) | 1.06 |
| Primary inductance $L_p$ (μH) | 32.4 |
| π capacitor $C_{n1}$, $C_{n2}$ (μF) | 1.0 |
| π inductance $L_n$ (μH) | 31.6 |
| Mutual inductance M (μH) | 10 |
| Secondary capacitor $C_s$ (μF) | 1.03 |
| Secondary inductance $L_s$ (μH) | 32.4 |

region in Fig. 7 demonstrates the voltage-stabilizing performance waveform during 0.01~0.02 sec after load change when the overshoot has been within the range of ±1 V during the short adjustment process. When load changes, the controller has restrain voltage fluctuation effectively within the overall voltage-stabilizing range, showing good control performance and satisfying the requirement of control accuracy.

When an ICPT system is under operation, it will meet disturbance from the input source. To verify the inhibitory action of the neural network controller under input disturbance, a 50 V DC disturbance was added to the dc source at t = 0.01 sec. Figure 8 shows the simulation waveform of output voltage. When the system was under input disturbance, the output voltage waveform became steady after an overshoot of 0.004 sec with the help of the neural network controller. The overshoot is small and the waveform is quickly stabilized. Besides, the system had fast response speed and kept amplitude of voltage error within the range of ±0.6 V at the steady state. Hence, the neural network controller meet the requirement of accurately stabilize the output voltage.

These simulation results have proven that the neural network controller can effectively help the ICPT system to resist load change and input disturbance, showing small overshoot and strong adjustment performance and robustness of the output voltage-stabilizing curves. Thus, it is feasible to use the topology of the system and the neural network controller.

## EXPERIMENTAL DEMONSTRATION

Based on Fig. 6, an experimental ICPT system with neural network controller was built, as shown in Fig. 9.

The Buck circuit was used as the regulator to control the input voltage $E_{dc}$, with the value of filter inductance $L_a$ being 5 mH, the value of output capacitor $C_a$ 100 μF and the chopping frequency 20 kHz. The control circuit detected the secondary resonant voltage $U_{cs}$ and coupled back to the neural network controller via RF-Link. To facilitate the discrete data processing with DSP, the neural network controller was discretized. The TMS320F2812 was used as the main control unit to compute error, realize

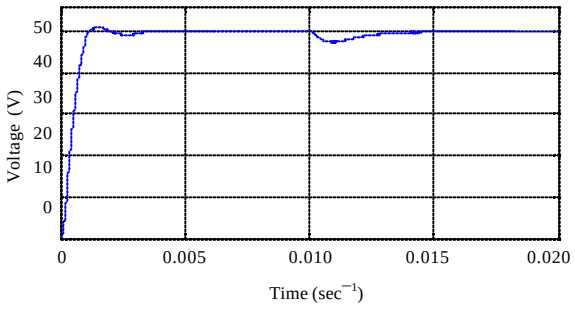


Fig. 8: Output voltage under input disturbance

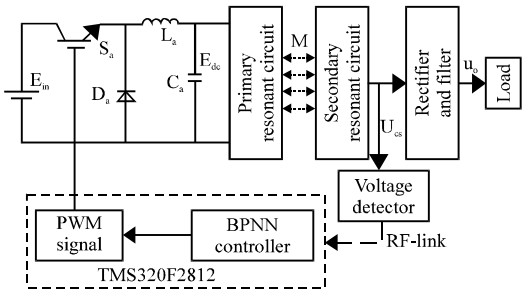


Fig. 9: Block diagram of experiment system

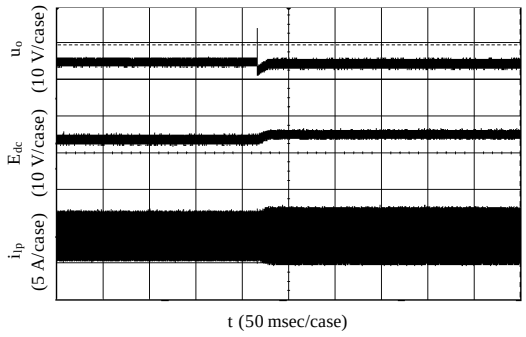


Fig. 10: Experiment waveforms when load jumped from 35-20 Ω

the neural network algorithm and calculate the duty cycle. The PWM signal was used to control the Buck circuit to adjust the output voltage.

To go a step further and validate the effect of neural network controller, two groups of load change was set in the experiment, including a resistance load transformed from 35-20 Ω and one transformed from 20-35 Ω. The expected output voltage of experiment system was assumed to be 13 V, while the input voltage $E_{in}$ was 30 V. The waveforms of output voltage of load $u_o$, control input voltage $E_{dc}$ and the primary current $i_{Lp}$ are shown in Fig. 10 and 11.

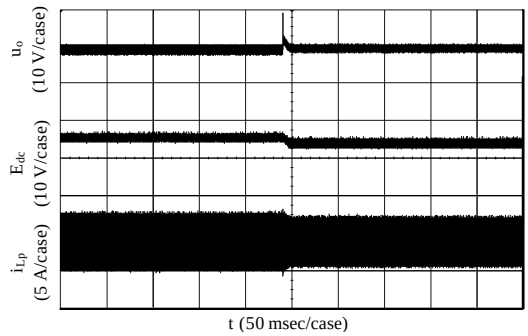


Fig. 11: Experiment waveforms when load jumped from 20-20 Ω

In Fig. 10, the secondary output voltage has been stabilized within 30 msec EC after an overshoot of 4 V due to the load change, that is to say, the overshoot is about 30%. In Fig. 11, the secondary output voltage reaches the given target state within 28 msec after an overshoot 3.6 V due to the load change, that is to say, the overshoot is about 28%. These two experiments demonstrate that when the system is under load disturbance, its secondary output voltage can be stabilized by this neural network controller with good control accuracy and robustness. Figure 10 and 11 also show that when the load becomes smaller, the primary input voltage $E_{dc}$ and the primary resonance current $i_{lp}$ become higher. However, when the load becomes bigger, the primary input voltage $E_{dc}$ and primary resonance current $i_{lp}$ will step down. These changes are caused by the variation of reflected impedance.

Moreover, as shown in Fig. 10 and 11, there are ripples in the waveforms of the secondary output voltage $u_o$ and the control input voltage $E_{dc}$. These ripples are caused by the input current disturbance due to the high frequency switching of the primary Buck circuit and inverter. Some measures can be taken to minify these ripples, such as filtering inductor and/or capacitor optimization and switching frequency optimization.

## CONCLUSIONS

This research studies the output voltage-stabilizing strategy for the ICPT system. As it is difficult to accurately model and effectively control the ICPT system due to its higher-order switch nonlinear behaviors, a neural network-based control strategy has been proposed. Compared with traditional models, the neural network has the feature of approximating complex nonlinear function. A feedforward neural network based on the BP algorithm has been designed. This neural network serves as the controller of the ICPT system to stabilize the output voltage. Based on the simulation analysis, it can be concluded that the proposed neural network controller can effectively and rapidly stabilize the output voltage which only shows small overshoot. This controller is not only accurate but also feasible. It can stabilize the output voltage even under parameter disturbance and load disturbance due to the self-learning ability and robustness. Furthermore, the load change experiments have verified that this neural network-based control strategy has great control effect and strong flexibility.

## ACKNOWLEDGMENTS

This research is financially supported by the National Natural Science Foundation of China (No. 51207173), the Chinese Research Fund for the Doctoral Program of Higher Education (No. 20100191120024) and the Postdoctoral Science Foundation of China (No. 20110490799). Authors also would like to give special thanks to the reviewers of this paper for their contributions to this study.

## REFERENCES

Abdalla, S.O. and S. Deris, 2005. Predicting protein secondary structure using artificial neural networks: Current status and future directions. Inform. Technol. J., 4: 189-196.

Bigdeli, N., K. Afshar, B.I. Lame and A. Zohrabi, 2008. Modeling of a five-link biped robot dynamics using neural networks. J. Applied Sci., 8: 3612-3620.

Cannon, B.L., J.F. Hoburg, D.D. Stancil and S.C. Goldstein, 2009. Magnetic resonant coupling as a potential means for wireless power transfer to multiple small receivers. IEEE Trans. Power Elec., 24: 1819-1825.

Chen, H.W., H.Z. Liu, X.W. Li, J.Q. Gao, R.G. Wei and Y. Shi, 2010. Experimental research on solids circulation rate in a double fluidized bed and BP neural network prediction. Proc. CSEE, 30: 25-29.

Coban, H., 2004. Application of an Artificial Neural Network (ANN) for the identification of grapevine (*Vitis vinifera* L.) genotypes. Asian J. Plant Sci., 3: 340-343.

Dai, X., K. Yu and Y. Sun, 2010. Study on H8 control method for CLC resonant inductive power transfer system. Proc. CSEE, 30: 47-54.

Dutta, M., P. Ghosh and J.K. Basu, 2012. Prediction of adsorption capacity of microwave assisted activated carbon for the decolorization of direct blue 86 by using artificial neural network. Asian J. Applied Sci., 5: 414-422.

Eriki, P.O. and R.I. Udegbunam, 2008. Application of neural network in evaluating prices of housing units in Nigeria: A preliminary investigation. J. Artif. Intell., 1: 21-27.

Hsieh, K.L., 2010. Employing artificial neural networks into achieving parameter optimization of multi-response problem with different importance degree consideration. Inform. Technol. J., 9: 918-926.

Hu, A.P., J.T. Boys and G.A. Covic, 2000. Frequency analysis and computation of a current-fed resonant converter for ICPT power supplies. Proceedings of the International Conference on Power System Technology, December 2000, Dept. of Electr. And Electron. Eng., Auckland Univ., Australia pp: 327-332.

Keshavarzi, A., F. Sarmadian, A.A. Zolfaghari and P. Pezeshki, 2012. Estimating water content at field capacity and permanent wilting point using non-parametric K-NN algorithm. Int. J. Agric. Res., 7: 166-168.

Li, H.L., A.P. Hu, G.A. Covic and C.S. Tang, 2009. A new primary power regulation method for contactless power transfer. Proceedings of the IEEE International Conference on Industrial Technology, February 10-13, 2009, Australia.

Li, Y.L., Y. Sun and X. Dai, 2012. Controller design for an uncertain contactless power transfer system. Informa. Technol. J., 8: 971-979.

Madawala, U.K. and D.J. Thrimawithana, 2011. Current sourced bi-directional inductive power transfer system. IET Power Electron., 4: 471-480.

Mao, Y.K., Z.C. Guan, L.M. Wang and B. Le, 2007. Prediction of leakage current of outdoor insulator based on BP artificial neural network. Proc. CSEE, 27: 7-11.

Moradewicz, A.J. and M.P. Kazmierkowski, 2010. Contactless energy transfer system with FPGA-controlled resonant converter. IEEE Trans. Ind. Electron., 57: 3181-3190.

Si, P., A.P. Hu, S. Malpas and D. Budgett, 2008. A frequency control method for regulating wireless power to implantable devices. IEEE Trans. Biomed. Cir. Syst., 2: 22-29.

Sun, Y., X. Lv, Z.H. Wang and C.S. Tang, 2012. A quasi sliding mode output control for inductively coupled power transfer system. Informa. Technol. J., 11: 1744-1750.

Tian, Y., Y. Sun, Y. Su, Z. Wang and C. Tang, 2012. Neural network-based constant current control of dynamic wireless power supply system for electric vehicles. Inform. Technol. J., 7: 876-883.

Valtchev, S., B. Borges, K. Brandisky and J.B. Klaassens, 2009. Resonant contactless energy transfer with improved efficiency. IEEE Trans. Power Electron., 24: 685-699.

Yugang, S., W. Zhihui, S. Yue and T. Chunsen, 2008. Modeling of contactless power transfer systems with a phase-shifted control method. Trans. China Elec. Soc., 23: 92-97.